





Article

Adsorption of crystal violet on kaolinite clay: kinetic and equilibrium study using non-linear models

Ali Boukhemkhem¹, Bamhammed Aissa-Ouaissi-Sekkouti², Jorge Bedia³ , Carolina Belver³
and Carmen B. Molina^{3*} 

¹Laboratory Interactions Materials – Environment (LIME), University of Mohamed Seddik Ben Yahia, Jijel, 18000, Algeria; ²Department of Process Engineering, University of Ammar Telidji, Laghouate, 03000, Algeria and ³Chemical Engineering Department, Faculty of Sciences, Universidad Autónoma de Madrid, Cantoblanco, 28049, Madrid, Spain

Abstract

This work studied the efficiency of Tamazert kaolinite clay for adsorbing the cationic dye crystal violet from an aqueous solution in a batch system. The kinetics of the process and the equilibrium of adsorption were studied using non-linear models. The characterization of Tamazert kaolinite clay showed that it has structural, textural and surface properties that are suitable for adsorption. The effects of various process parameters such as contact time, initial dye concentration, initial pH, adsorbent dose and temperature were tested. The kinetic study using non-linear regression showed that the pseudo-second order model best fitted the experimental data. The intra-particle model was also used to estimate the contribution of intra-particle diffusion to this process. The adsorption isotherms were fitted to Freundlich, Langmuir and Redlich–Peterson models, showing that the adsorption is limited to a monolayer with a monolayer adsorption capacity of 44.2 mg g⁻¹. The thermodynamic study indicated that the process is exothermic, spontaneous and accompanied by a decrease in entropy.

Keywords: adsorption, crystal violet, equilibrium, kinetics, Langmuir, Tamazert kaolinite clay, thermodynamics

(Received 6 April 2022; revised 14 August 2022; Accepted Manuscript online: 24 August 2022)

Water resources are affected significantly by pollution because many industrial sectors consume large amounts of fresh water (Pavan *et al.*, 2007; Sarma *et al.*, 2019; Yaseen *et al.*, 2019). In particular, the textile, paper, printing, leather, food and cosmetics industries generate substantial amounts of residual water charged with various kinds of organic pollutants. Among the most common pollutants are synthetic dyes, representing a significant hazard to both human health and the environment. Removal of these compounds from wastewater is essential because of the complex nature of aromatic structures that renders them highly stable in aqueous environments (Mobarak *et al.*, 2018; Mouni *et al.*, 2018). Their refractory nature, even at low concentrations, is the source of many problems such as blocking sunlight and oxygen penetration into aquatic systems, thus harming the aquatic flora by inhibiting photosynthesis. Furthermore, they represent a potential hazard to human health due to their aromatic structures, which render them mutagenic and carcinogenic (Li *et al.*, 2017; Benhabiles *et al.*, 2021).

Crystal violet (CV) is a cationic dye, and it is one of the most common dyes used in the textile, paper, printing and paint industries. In addition, it is used widely as a biological stain and dermatological agent in human and veterinary medicine (Monash *et al.*, 2011; Puri *et al.*, 2018; Sarabandan *et al.*, 2019a). Considered a

carcinogen, mutagen and toxic, CV can also cause some other harmful effects at higher concentrations, such as blindness, digestive system issues, skin irritation and respiratory and kidney failure. Therefore, it represents a significant hazard to human health; wastewater containing this dye must be treated effectively before its reuse or discharge into the aquatic medium (Puri *et al.*, 2018; Abbasi *et al.*, 2020; Rezazadeh *et al.*, 2021).

Many techniques have been developed to eliminate dyes from wastewater, including biological processes (Varjani *et al.*, 2020; Srinivasan *et al.*, 2021), advanced oxidation processes (Miklos *et al.*, 2018), photochemical degradation (Darghazadeh *et al.*, 2018), electrochemical degradation (Belal *et al.*, 2021), chemical coagulation–flocculation (Gadekar *et al.*, 2016), nanofiltration with membranes (Askari *et al.*, 2016), reverse osmosis (Al-Bastaki, 2004) and adsorption (Sharma *et al.*, 2011; Yagub *et al.*, 2014). The latter method has attracted great attention because of its high efficiency, low cost, simple and clean operation and low energy input required for treating dye wastewaters effectively (Nadaroglu *et al.*, 2015; Khairy *et al.*, 2018; Boukhemkhem *et al.*, 2020). Activated carbon is the most widely used industrial-scale commercial adsorbent due to its effectiveness and versatility, large specific surface area and diversity of functional groups (Giannakoudakis *et al.*, 2016). However, it has some disadvantages, such as its high cost and difficulties regarding regeneration and separation. Thus, its use is uneconomical for industrial applications, and researchers seek lower-cost, naturally available, reusable and environmentally friendly alternative materials (Nandi *et al.*, 2008; Liew *et al.*, 2018).

*E-mail: carmenbelen.molina@uam.es

Cite this article: Boukhemkhem A, Aissa-Ouaissi-Sekkouti B, Bedia J, Belver C, Molina CB (2022). Adsorption of crystal violet on kaolinite clay: kinetic and equilibrium study using non-linear models. *Clay Minerals* 57, 41–50. <https://doi.org/10.1180/clm.2022.18>

Alternative adsorbents have been used, such as biomass wastes (Ali *et al.*, 2008; Kumar *et al.*, 2011; Kulkarni *et al.*, 2017; Abbasi *et al.*, 2020), fly ash (Liew *et al.*, 2018), natural and synthetic zeolites (Rida *et al.*, 2013; Sarabadan *et al.*, 2019b), alumina (Banerjee *et al.*, 2019) and mesoporous and microporous silica (Jiang *et al.*, 2019; Hachemaoui *et al.*, 2020). Clay minerals have attracted the attention of researchers due to their natural origin, low cost, high availability and good adsorbent properties. Various clay minerals have been used for the removal of dyes from wastewater, such as pyrophyllite (Miyah *et al.*, 2017), smectite (Rytwo *et al.*, 1993; Hamza *et al.*, 2018; Puri *et al.*, 2018; Sarabadan *et al.*, 2019a; Intachai *et al.*, 2021), ball clay (Monash *et al.*, 2011), clinoptilolite (Nadaroglu *et al.*, 2015), kaolinite (Sargin *et al.*, 2013), sepiolite (Eren *et al.*, 2007; Karatas *et al.*, 2018) and palygorskite (Al-Futaisi *et al.*, 2007). Kaolinite clay (KT) is one of the cheapest, most naturally available and non-toxic of such materials. However, its small specific surface area ($<20 \text{ m}^2 \text{ g}^{-1}$) and low cation-exchange capacity (CEC; $\sim 12 \text{ meq } 100 \text{ g}^{-1}$) make it less attractive than other clays for adsorption processes (Nandi *et al.*, 2008; Jiang *et al.*, 2009; Boukhemkhem *et al.*, 2017). The literature reports few cases of the use of KT as an adsorbent for the removal of only methylene blue (MB) dye as a cationic dye, and the most attractive clays were natural or modified montmorillonites due to their large CEC and swelling properties, which make them suitable for intercalation by some surfactants (Rytwo *et al.*, 1993; Sarabadan *et al.*, 2019a, 2021). In previous research on KT, Rida *et al.* (2013) evaluated the adsorption performance of MB removal in comparison with 4A zeolite. Boukhemkhem *et al.* (2017) tested several treatments to improve the adsorption capacity of KT for MB. Recently, Mouni *et al.* (2018) also studied the adsorption of MB on KT.

There are no studies in the literature focusing on the use of Tamazert KT as an adsorbent for the removal of other cationic dyes such as CV. Therefore, we studied the efficiency of KT for absorbing other cationic dyes. Furthermore, previous work has used linear models to study the kinetic parameters and equilibrium of adsorption of such processes, but one could criticize the use of the linear forms of such models, especially for the pseudo-second order (PSO) kinetic model, because when the linear form of the PSO model is considered it always gives good linearity with a high determination coefficient (Bujdak, 2020). Therefore, the present work analyses the removal efficiency of KT for the cationic dye CV by studying the effects of various parameters, including contact time, initial dye concentration, initial pH, adsorbent dose and temperature. The kinetic mechanism was evaluated using the non-linear forms of the pseudo-first order (PFO) and PSO models. The equilibrium of adsorption was also studied using the non-linear forms of the Langmuir, Freundlich, Langmuir–Freundlich and Redlich–Peterson models.

Materials and methods

Chemical reagents

The Tamazert KT was provided by the National Society of Ceramics, located in the province of Jijel (western Algeria), and it was used as received. All chemicals used in this study, including concentrated hydrochloric acid (HCl, 37 wt.%), sodium hydroxide (NaOH), sodium chloride (NaCl) and CV ($\text{C}_{25}\text{H}_{30}\text{ClN}_3$), were of analytical grade and were purchased from Sigma-Aldrich (MO, USA). The initial pH values of all of the solutions were adjusted with a 0.1 M solution of HCl or NaOH. Solutions with the desired

concentrations were obtained by appropriate dilution of the initial solution (200 mg L^{-1}) of CV dye. All solutions were prepared with deionized water.

Characterization techniques

Chemical composition. The chemical composition was determined using inductively coupled plasma spectroscopy with an ICP 5000 DV spectrometer (PG Instruments, UK).

X-ray diffraction. The powder X-ray diffraction (XRD) trace of the sample was recorded on a Philips (The Netherlands) X'pert diffractometer using $\text{Cu-K}\alpha$ radiation in the range of $5\text{--}90^\circ 2\theta$ at a scanning speed of $0.02^\circ 2\theta \text{ s}^{-1}$.

Fourier-transform infrared spectroscopy. The Fourier-transform infrared (FTIR) spectrum was recorded using a Shimadzu (Japan) IRAffinity-1 spectrometer in the range of $400\text{--}4000 \text{ cm}^{-1}$. The samples were prepared using the KBr technique by mixing 200 mg of KBr with 1 mg of powdered clay using a pelletizer.

Thermal analysis. Thermal gravimetric analysis (TGA) and differential thermal analysis (DTA) were conducted in the temperature range of $298\text{--}1223 \text{ K}$ using PerkinElmer (MA, USA) TGA7 and DTA7 devices.

Scanning electron microscopy. The morphological features of the KT were identified using scanning electron microscopy (SEM) with a Philips XL20 scanning electron microscope at an accelerating voltage of 20 kV. Samples were coated previously using an Edwards (UK) Auto 306 vacuum coater with carbon adhesive tabs and silver as the coating agent.

Textural properties

Textural properties were determined using N_2 adsorption-desorption at 77 K with a Micromeritics (GA, USA) Tristar 3020 instrument. Before the analysis, samples were outgassed overnight at 150°C and 5.10^{-3} Torr . The specific surface area was calculated from the Brunauer–Emmett–Teller (BET) equation in the linear portion at 0.05–0.35 relative pressure. The micropore volume was determined using the *t*-plot method. The pore-size distribution was calculated from desorption data using the Barret–Joyner–Halenda (BJH) method (Li *et al.*, 2010).

The point of zero charge (pH_{pzc}) was calculated using the pH drift method in which 0.2 g of sample was added to 0.04 L of 0.1 M NaCl solution with pH varying from 2 to 12 and then stirred for 24 h. The values of $\text{pH}_f - \text{pH}_i$ against pH_i were plotted (whereby pH_f is the final pH and pH_i is the initial pH), with the pH_{pzc} being the pH at which $\text{pH}_f - \text{pH}_i = 0$ (Feng *et al.*, 2009). Solution pH measurements were carried out using a HI 223 pH meter (Hanna Instruments, Hungary).

Cation-exchange capacity

The CEC of the KT clay was determined using the MB spot method: 1 g of sample was added to 0.015 L of water under vigorous stirring until the sample had dispersed. Then, 0.015 L of H_2O_2 (3%) with 12 drops of H_2SO_4 (2.5 M) were added to the previous suspension. The resulting suspension was boiled for 10 min and diluted with 0.02 L of water. Next, an MB solution (3.2 g L^{-1}) was added in 0.001 L increments. After each addition, the solution was stirred vigorously for at least 20 s using a magnetic stirrer hotplate MS7-H550-Pro (Scilogex, CT, USA). Then, a drop of the sample was removed from the end of the stirring

rod. The approximate end point was obtained when a blue ring spread out from the blue spot on the filter paper. Equation 1 was used for the calculation of the CEC (meq 100 g⁻¹; Boukhemkhem *et al.*, 2017):

$$\text{CEC} = \frac{V_{\text{MB}}}{W} \quad (1)$$

where V_{MB} is the added volume of MB dye (mL) and W is the weight of the sample (g).

Acidity and basicity

The acidity and basicity of the KT were evaluated using standard Boehm titration as follows: 0.25 g of each sample was mixed with 0.05 L of aqueous reactant solution (0.01 mol L⁻¹ HCl or NaOH). The mixtures were stirred for 24 h at a constant speed and at room temperature. Then, the suspensions were submitted to filtration and centrifugation to obtain a clean supernatant that was titrated in the presence of phenolphthalein indicator (Issa *et al.*, 2014).

Adsorption experiments

Batch adsorption experiments were performed using 0.05 L dye solution for the kinetic study and by adding the KT to the CV solution (40 mg L⁻¹) for 2 h to reach equilibrium for the parameter effect and equilibrium studies. After each experiment, the solid was recovered using centrifugation and the residual dye concentration was determined using ultraviolet–visible spectroscopy (Optizen 2120 equipment; Mecasys, Republic of Korea) fixing the λ_{max} at 590 nm. The decolourization efficiency was calculated using Equation 2:

$$(\%) \text{ Decolourization} = \left(1 - \frac{C_e}{C_0}\right) \times 100 \quad (2)$$

where C_0 (mg L⁻¹) is the initial dye concentration and C_e (mg L⁻¹) is the dye concentration at equilibrium. The adsorption capacity at any time (t) and at equilibrium were calculated using Equations 3 and 4, respectively:

$$q_t = \frac{V}{m}(C_0 - C_t) \quad (3)$$

$$q_e = \frac{V}{m}(C_0 - C_t) \quad (4)$$

where q_t (mg g⁻¹) is the adsorption capacity at any time, q_e (mg g⁻¹) is the adsorption capacity at equilibrium, V is the solution volume (L) and m is the adsorbent dose (g L⁻¹).

The effect of the adsorbent dosage was studied by varying the amount of KT added from 0.2 to 8.0 g L⁻¹. The stirring speed was varied from 25 to 600 rpm, setting the CV and KT concentrations at 40 mg L⁻¹ and 1 g L⁻¹, respectively. The effect of the initial pH was tested in the pH range of 3–9 using an adsorbent dose of 1 g L⁻¹. The kinetic study was performed using a KT load of 1 g L⁻¹ with various initial concentrations (10, 20, 30 and 40 mg L⁻¹) using 0.2 L of dye solution. The adsorption isotherms were constructed at 290, 303 and 313 K.

Table 1. Chemical composition and textural and surface properties of the KT.

Property	Value
<i>Chemical composition (wt.%)</i>	
SiO ₂	50.27
Al ₂ O ₃	33.06
K ₂ O	2.28
Fe ₂ O ₃	1.14
CaO	0.56
TiO ₂	0.50
NaO	0.40
MgO	0.33
<i>Mineralogical composition (wt.%)</i>	
Kaolinite	76
Quartz	10
Muscovite	8
Anatase	2
Other minerals	4
<i>Particle size (%)</i>	
>40 μm	1
2–10 μm	49
<2 μm	30
<i>Textural properties</i>	
S _{BET} (m ² g ⁻¹)	14
S _{EXT} (m ² g ⁻¹)	12
S _{mic} (m ² g ⁻¹)	2
V _p (cm ³ g ⁻¹)	0.055
V _{mic} (cm ³ g ⁻¹)	0.0011
<i>Surface properties</i>	
CEC (meq 100 g ⁻¹)	12
Acidity (mmol g ⁻¹)	1.70
Basicity (mmol g ⁻¹)	0.02
pH _{pzc}	3.1

S_{BET} = BET-specific surface area; S_{EXT} = external specific surface area; S_{mic} = micropore-specific surface area; V_{mic} = micropore volume; V_p = total pore volume.

Results and discussion

Adsorbent characterization

The KT is composed of mainly Si and Al (Table 1) with the presence of minor K, Fe, Na, Ti and Mg ranging between 0.2 and 1.9 wt.%. This composition agrees with the composition of kaolins (Feng *et al.*, 2009; Konan *et al.*, 2009; San Cristobal *et al.*, 2010). Figure 1a shows the XRD trace of the KT. According to the Joint Committee on Powder Diffraction Standards (JCPDS) database, the presence of kaolinite as the main phase is observed with its characteristic peak at 12.4°2θ. Impurities such as muscovite (8.8°2θ), anatase (25.2°2θ) and quartz (26.5°2θ) were also detected. The mineralogical composition of this KT and the approximate particle-size range (both supplied by the manufacturer) are also included in Table 1. The clay consists of mostly kaolinite (76 wt.%) and minor quartz (10 wt.%) and muscovite (8 wt.%).

Figure 1b shows the FTIR spectrum of the KT, which is characterized by the presence of bands assigned to hydroxyl groups at 3446 (OH stretching in adsorbed water), 3620, 3649 and 3698 cm⁻¹ (OH stretching in kaolinite). The water bending band was observed at 1674 cm⁻¹ (Boukhemkhem *et al.*, 2017). The band at 912 cm⁻¹ is attributed to Al–OH bending in kaolinite. Bands located at 1115, 1032, 1006 and 740 cm⁻¹ correspond to the Si–O–Si bonds characteristic of the kaolinite structure. The presence of Si–O–Al bonds is observed at 795, 754, 696, 671, 536 and 471 cm⁻¹ (Volzone *et al.*, 2006; San Cristóbal *et al.*, 2010; Hassen *et al.*, 2011; Boukhemkhem *et al.*, 2017).

The TGA-DTA curves exhibit two endothermic events (Fig. 2). The first one, at 393 K, is attributed to the evaporation of

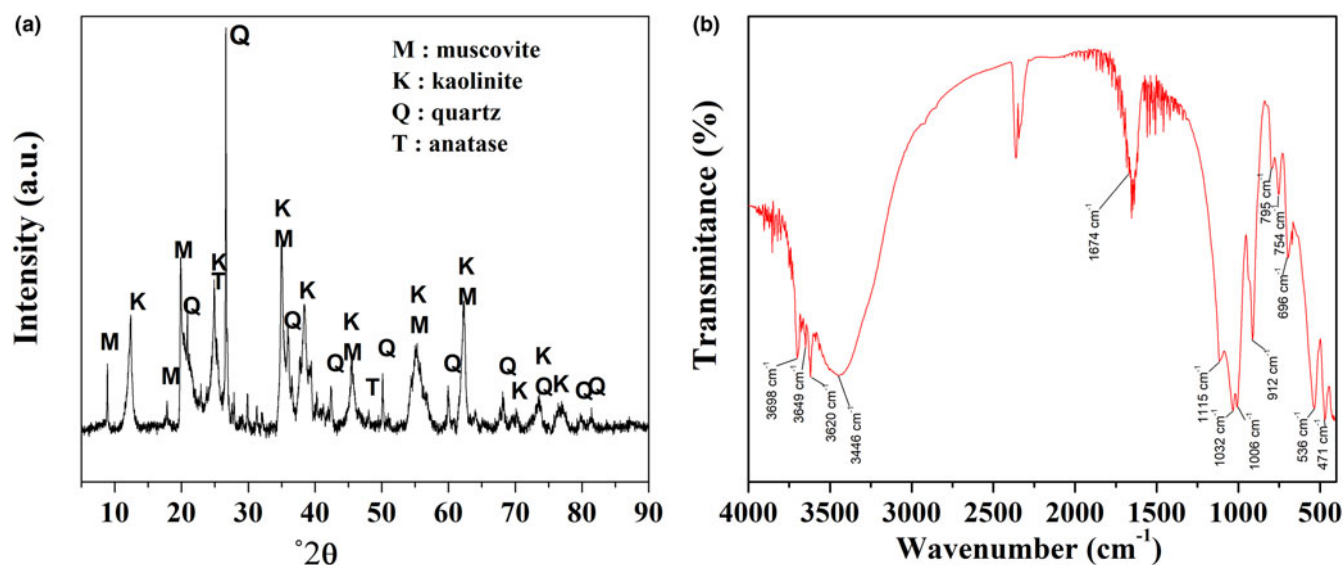


Fig. 1. (a) XRD trace and (b) FTIR spectrum of the KT.

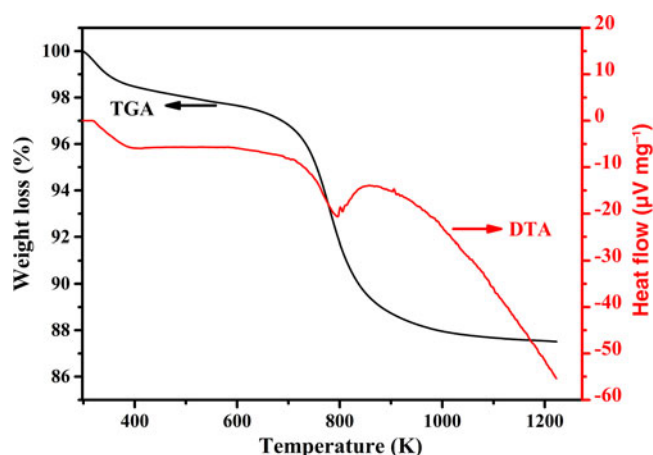


Fig. 2. TGA and DTA curves for the KT.

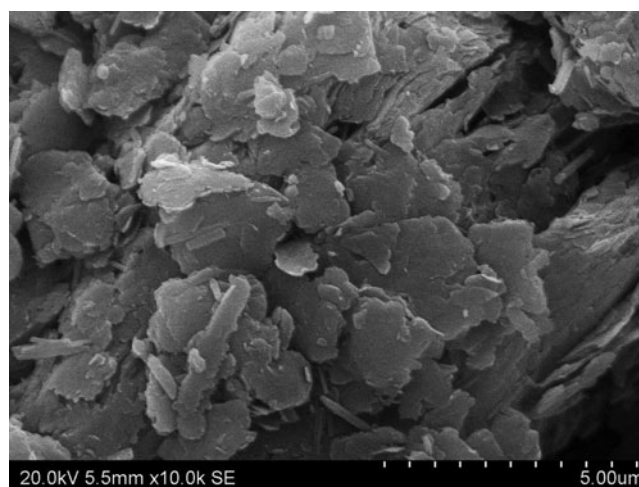


Fig. 3. SEM image of the KT.

hydration water with a small weight loss of $\sim 4.0\%$. The second event at 793 K, which is of greater intensity, is attributed to the dehydroxylation and conversion of kaolinite into metakaolinite, with a weight loss of $\sim 10.5\%$. The theoretical weight loss for pure kaolinite is 13.8% according to the following reaction: $\text{Si}_2\text{Al}_2\text{O}_5(\text{OH})_4 \rightarrow \text{Si}_2\text{Al}_2\text{O}_7 + 2\text{H}_2\text{O}$. This difference between these two weight-loss values is attributed to the presence of impurities, mainly quartz and muscovite (Volzone *et al.*, 2006; Muayad *et al.*, 2015).

The SEM images revealed the presence of kaolinite layers forming stacked sheets of variable thickness (Fig. 3). In addition, kaolinite aggregates are also present (Boukhemkhem *et al.*, 2017; Sarma *et al.*, 2019).

The textural properties were determined using N_2 adsorption-desorption (Fig. 4a). The isotherm belonged to type IV with a H3 hysteresis loop, which is characteristic of predominantly mesoporous materials (Thommes *et al.*, 2015). This type of isotherm is typical of aggregates of plate-like particles such as clay minerals (Abraham *et al.*, 2019). Moreover, the pore-size distribution is characterized by a unimodal distribution centred

at 3.59 nm (Fig. 4b) belonging to the mesoporosity interval (Boukhemkhem *et al.*, 2019).

The BET surface area of the KT is $14 \text{ m}^2 \text{ g}^{-1}$ (Table 1), which is in good agreement with previous studies on KTs (Nandi *et al.*, 2008; Fabbri *et al.*, 2013; Sarma *et al.*, 2019). Furthermore, the CEC of the KT is 12 meq 100 g^{-1} (Table 1). This low value is mainly due to the absence of a layer charge and exchangeable cations in the interlayer space, as the KT has only external ions generated by silanol (Si-OH) and aluminol (Al-OH) groups (de Lima *et al.*, 2010). The acidic-basic properties of the KT indicate its high acidity (1.70 mmol g^{-1}), which is due to the presence of Si-OH and Al-OH groups capable of accepting or releasing protons. This acidic character was relevant as the protons can be released easily due to the high electronegativity of the oxygen atoms in comparison with the hydrogen atoms. The pH_{pzc} of the KT was 3.1; hence, the KT holds a positive charge at pH_i values lower than 3.1 and a negative charge at pH_i values greater than this figure.

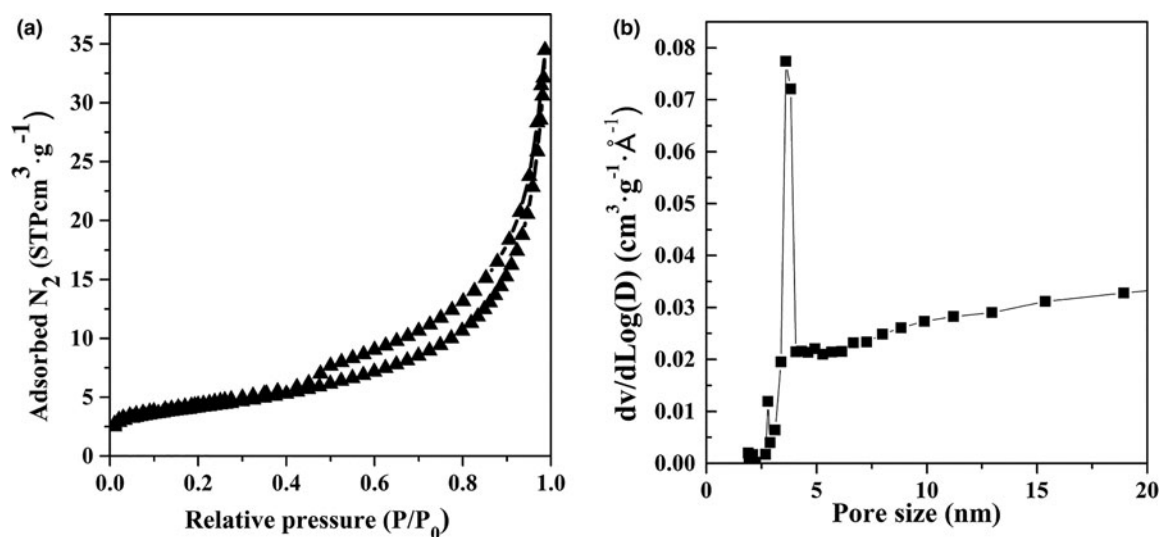


Fig. 4. (a) N_2 adsorption-desorption isotherm and (b) pore-size distribution of the KT. STP = standard temperature and pressure.

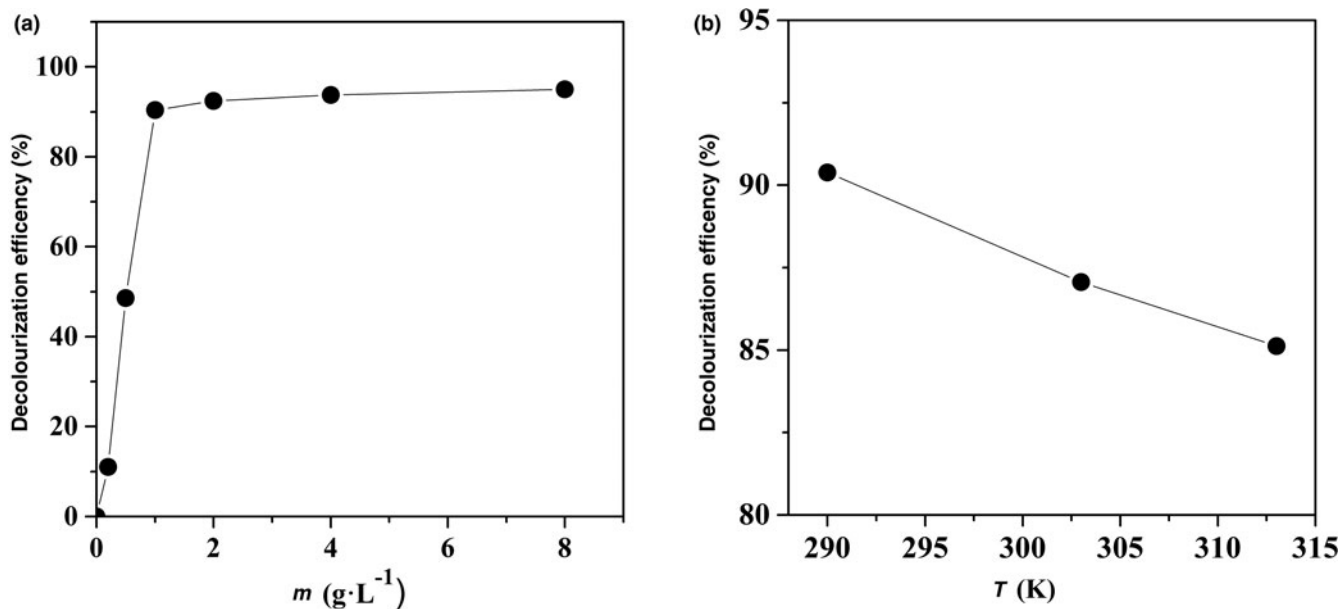


Fig. 5. Effect on the decolourization efficiency of (a) the adsorbent dose ($C_0 = 40 \text{ mg L}^{-1}$, $pH_i = 5.6$, stirring speed = 400 rpm, $t = 290 \text{ K}$, $V = 0.05 \text{ L}$, contact time = 2 h) and (b) temperature ($C_0 = 40 \text{ mg L}^{-1}$, adsorbent dose = 1 g L^{-1} , $pH_i = 5.6$, stirring speed = 400 rpm, $V = 0.05 \text{ L}$, contact time = 2 h).

Adsorption study

Effects of experimental parameters. The effect of adsorbent dose on dye removal is shown in Fig. 5a. The increase of the adsorbent dose from 0.2 to 1.0 g L^{-1} affected CV removal significantly; it increased from 11% to 90%. This is due to increases in the number of adsorption active sites and the available surface area with increasing adsorbent dose. Doses $>1 \text{ g L}^{-1}$ did not affect CV adsorption, which remained almost constant, as most of CV molecules were adsorbed and very few remained in the solution (Kulkarni *et al.*, 2017). For this reason, an adsorbent dose of 1 g L^{-1} was used in the subsequent tests.

Increasing the temperature (290 – 313 K) had a negative effect on the adsorption of CV, which decreased from 89% to 85%

(Fig. 5b). Thus, the adsorption of CV on the KT may be exothermic in nature due to the weakness of the physical bonds between the CV cations and the outer hydroxyl groups (Nandi *et al.*, 2008).

The effect of stirring speed on CV removal is illustrated in Fig. 6a. Dye removal increased from 66% to 90% when the stirring speed increased from 25 to 400 rpm. This is due to a reduction in the film boundary layer surrounding the KT particles, leading to a significant improvement in the external film transfer and consequently in the percentage of dye removal (Geethakarathi *et al.*, 2011). Further increases in stirring speed did not affect dye removal. Thus, 400 rpm was selected as the optimal stirring speed for the rest of the study.

The initial pH of the dye solution is very important for adsorption as it influences the dye-removal efficiency of clays, affecting

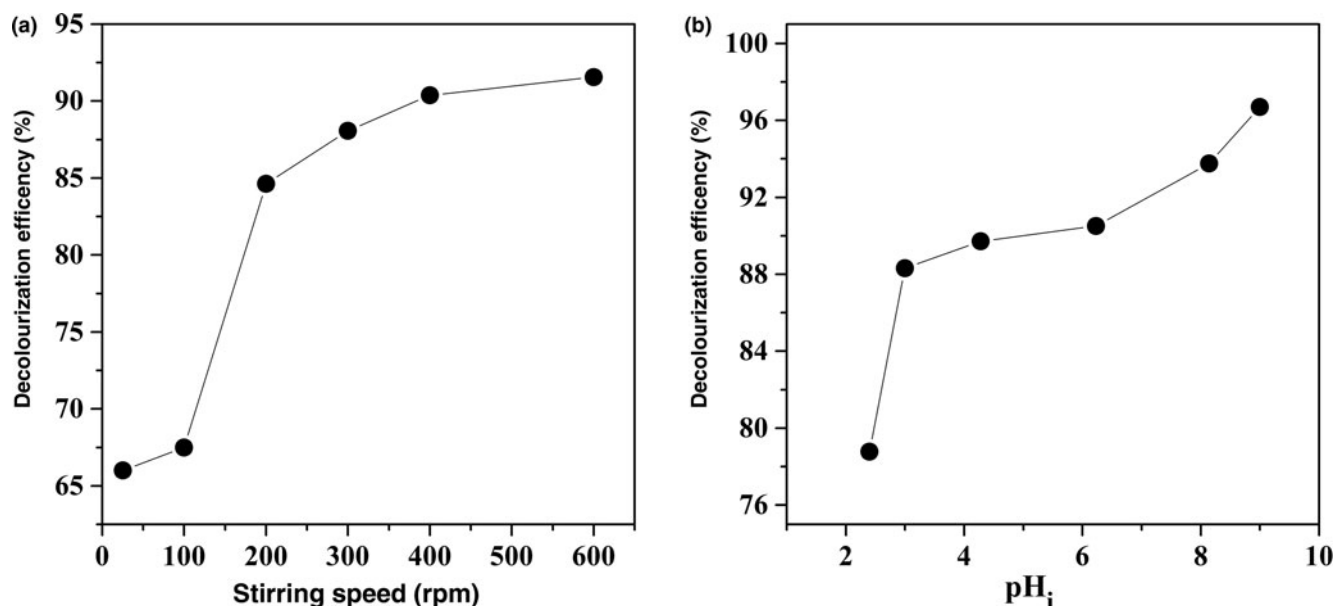


Fig. 6. Effect on the decolourization efficiency of (a) stirring speed ($C_0 = 40 \text{ mg L}^{-1}$, adsorbent dose = 1 g L^{-1} , $pH_i = 5.6$, $t = 290 \text{ K}$, $V = 0.05 \text{ L}$, contact time = 2 h) and (b) pH_i ($C_0 = 40 \text{ mg L}^{-1}$, adsorbent dose = 1 g L^{-1} , stirring speed = 400 rpm, $t = 290 \text{ K}$, $V = 0.05 \text{ L}$, contact time = 2 h).

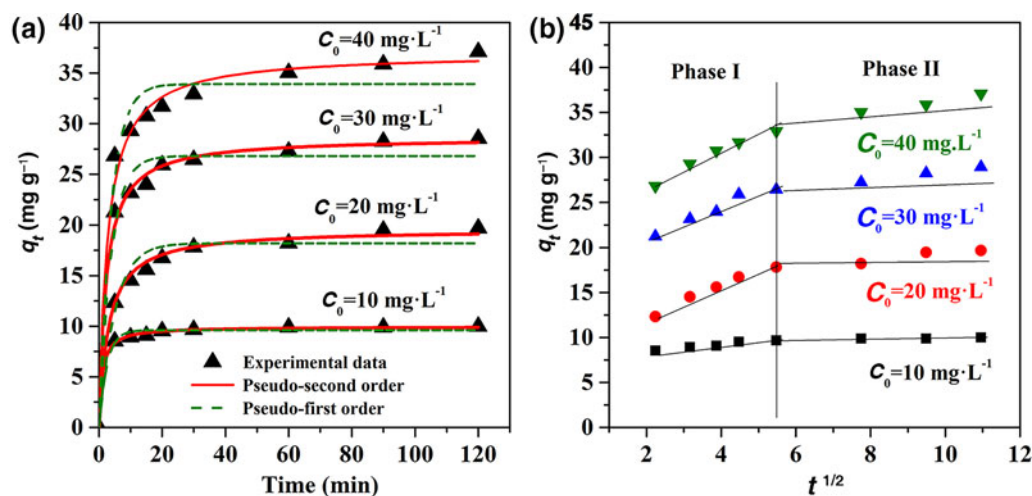


Fig. 7. (a) Adsorption on the KT at various initial concentrations of CV and fitting to PFO and PSO models. (b) Non-linear fitting for the adsorption of CV on the KT at various initial dye concentrations using the intra-particle diffusion model (adsorbent dose = 1 g L^{-1} , $pH_i = 9.0$, $t = 290 \text{ K}$, $V = 0.2 \text{ L}$, stirring speed = 400 rpm).

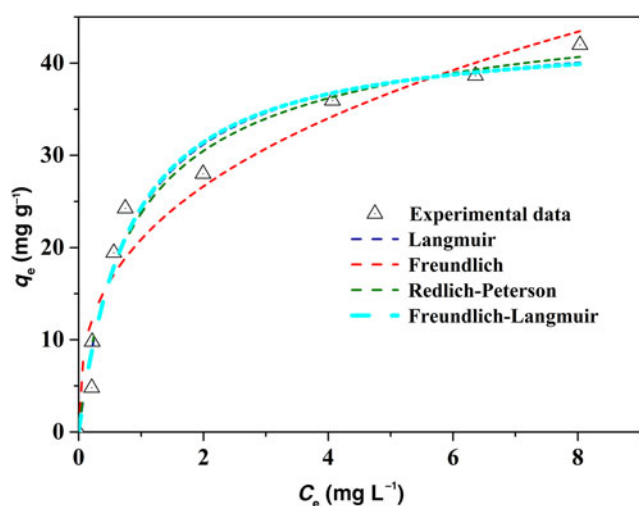
the charges of both the dye molecule and the clay surface. The increase of the initial pH from 2.4 to 9.0 and especially above the pH_{pzc} increased significantly the dye-removal efficiency from 78% to 96% (Fig. 6b). This is mainly due to an increase in the electrostatic forces between the negatively charged clay surface and the positively charged dye molecule. However, at pH_i values lower than the pH_{pzc} the dye-removal percentage decreased due to repulsive forces between the dye molecules holding a positive charge and the positively charged clay surface. Furthermore, some competition for the active sites might exist between dye molecules and protons (Hamza *et al.*, 2018). Thus, a pH_i value of 9.0 was selected for the subsequent studies.

Kinetic study. The kinetic study was performed using the optimum values of the parameters studied previously. Curves representing the evolution of the adsorbed CV quantity as a function of time are illustrated in Fig. 7a.

CV adsorption increased from 10 to 37 mg g^{-1} with increasing initial dye concentration from 10 to 40 mg L^{-1} . The increase in the amount adsorbed at greater dye concentrations can be explained by the greater number of dye molecules in the liquid phase, which increases adsorbent-adsorbate interactions, resulting in greater adsorption. Furthermore, the adsorption is rapid during the first 5 min of the process for all concentration values due to the high level of availability of free adsorption sites at the beginning of the process. However, the progressive saturation of vacant sites decreased the adsorption rate gradually until equilibrium was reached. The experimental data shown in Fig. 7a were fitted to three well-known kinetic models: the PFO model, the PSO model (both shown in Fig. 7a) and the intra-particle diffusion model (Fig. 7b). The non-linear forms of the PFO and PSO models were chosen as the use of their linear forms has been criticized in the literature (Lin *et al.*, 2009; Xia *et al.*, 2018; Bujdak, 2020).

Table 2. Kinetic parameters of CV adsorption on the KT following various kinetic models.

C_0 (mg L ⁻¹)	$q_{e,exp}$ (mg g ⁻¹)	PFO model			PSO model			Intra-particle diffusion model		
		k_1 (min ⁻¹)	q_e (mg g ⁻¹)	R^2	k_2 (g mg ⁻¹ min ⁻¹)	q_e	R^2	k_{int} (mg g ⁻¹ min ^{-0.5})	I (mg g ⁻¹)	R^2
10	9.97	0.408	9.61	0.987	0.104	9.95	0.997	0.365	7.739	0.942
20	19.66	0.202	18.19	0.970	0.017	19.57	0.994	1.508	8.900	0.976
30	28.53	0.267	26.81	0.966	0.016	28.85	0.994	1.668	17.738	0.940
40	37.08	0.265	33.91	0.960	0.010	36.98	0.985	1.874	23.086	0.958

**Fig. 8.** Adsorption isotherm of CV on the KT and non-linear fitting to various models (adsorbent dose = 1 g L⁻¹, pH_i = 9.0, $t = 290$ K, $V = 0.05$ L, stirring speed = 400 rpm).

The equations for these three models are as follows:

$$q_t = q_e(1 - e^{-k_1 t}) \quad (5)$$

where q_t and q_e (mg g⁻¹) are the adsorption capacities at time t (min) and at equilibrium, respectively, and k_1 (min⁻¹) is the PFO rate constant;

$$q_t = \frac{k_2 q_e^2 t}{1 + k_2 q_e t} \quad (6)$$

where q_t and q_e (mg g⁻¹) are the adsorption capacities at time t (min) and at equilibrium, respectively, and k_2 (g mg⁻¹ min⁻¹) is the PSO rate constant; and

$$q_t = k_{int} t^{1/2} + I \quad (7)$$

where q_t (mg g⁻¹) is the adsorption capacity at time t (min), k_{int} (mg g⁻¹ min^{-0.5}) is the intra-particle diffusion model constant and I (mg g⁻¹) is the intercept.

The PFO model did not describe adequately the kinetics of CV adsorption, whereas the PSO model was best able to describe the uptake of CV on the KT, as the corresponding coefficients of determination were closer to unity in comparison with those obtained from the other models (Fig. 7a & Table 2). Furthermore, a decrease in k_2 values with increasing initial CV concentration was observed (Table 2). This reveals that at low initial CV concentrations the adsorption rate was important due to the high level of accessibility of the free adsorption sites for all of

the dye molecules and there being no competition between the molecules (Nandi *et al.*, 2008; Nasuha *et al.*, 2011; Auta *et al.*, 2012). Moreover, adsorption occurred on active sites located on the adsorbent surface, which could be reached easily by the adsorbate molecules. However, increasing the initial adsorbate concentration increased the competition between dye molecules, and when the most accessible adsorption sites on the adsorbent surface were occupied, the molecules diffused to the vacant sites in the pores and consequently the adsorption rate slowed down (Vishwakarma *et al.*, 2018).

The graphical representation of the intra-particle diffusion model indicates the presence of two linear regions (Fig. 7b). The first one is attributed to intra-particle diffusion and the second one is attributed to the establishment of equilibrium. The first linear trend did not pass through the origin for all of the concentrations. These results suggest that once the active sites located on the surface are saturated, dye molecules reach the active sites within the mesopores until all are saturated and equilibrium is reached.

Moreover, k_{int} increased from 0.365 to 1.874 mg g⁻¹ min^{-0.5} with the CV concentration increasing initial from 10 to 40 mg g⁻¹. This may be ascribed to an increase in the concentration gradient, making the diffusion within pores more important. This result was also confirmed by the I values, which increased from 7.739 to 23.086 mg g⁻¹, suggesting that the number of CV molecules increased on the boundary layer (Hamdaoui *et al.*, 2007). However, intra-particle diffusion was not the only limiting step in terms of the control of the rate of adsorption because external diffusion through the boundary layer also interfered with this control.

Equilibrium study. Four models were used to describe the equilibrium data obtained from the adsorption isotherm of CV on the KT: the Langmuir (Equation 8), Freundlich (Equation 9), Redlich–Peterson (Equation 10) and Langmuir–Freundlich models (Equation 11) (Amari *et al.*, 2010; Sarabadan *et al.*, 2019b). They are used in their non-linear forms to avoid linearization errors in the determination of the regression coefficient (R^2):

$$q_e = \frac{q_m K_L C_e}{1 + K_L C_e} \quad (8)$$

$$q_e = K_F C_e^{1/n} \quad (9)$$

$$q_e = \frac{K_{RP} C_e}{1 + \alpha_{RP} C_e} \quad (10)$$

$$q_e = \frac{q_{mLF} (K_{LF} C_e)^{m_{LF}}}{1 + (K_{LF} C_e)^{m_{LF}}} \quad (11)$$

Table 3. Fitting parameters using various adsorption isotherm models.

Model	Parameters			
Freundlich	$K_F ((\text{mg g}^{-1}) \cdot (\text{mg L}^{-1})^{-1/n})$	n	R^2	
	20.88	0.351	0.936	
Langmuir	$q_m (\text{mg g}^{-1})$	$K_L (\text{L mg}^{-1})$	R^2	
	44.19	1.200	0.971	
Redlich–Peterson	$K_{RP} (10^{-3} \text{ L g}^{-1})$	$\alpha_{RP} (10^{-3} \text{ L mg}^{-1})^\beta$	β	R^2
	59.68	1.518	0.941	0.968
Langmuir–Freundlich	$q_{mLF} (\text{mg g}^{-1})$	$K_{LF} (\text{L mg}^{-1})$	m_{LF}	R^2
	43.51	1.254	1.037	0.967

Table 4. Thermodynamic parameters for the adsorption of CV onto the KT.

Temperature (K)	$\Delta H^\circ (\text{kJ mol}^{-1})$	$\Delta S^\circ (\text{J K}^{-1} \text{mol}^{-1})$	$\Delta G^\circ (\text{kJ mol}^{-1})$
290	-11.56	-0.022	-5.17
303			-4.89
313			-4.67

where C_e is the dye concentration at equilibrium (mg L^{-1}), q_e is the adsorbed quantity of CV at equilibrium (mg g^{-1}), q_m is the monolayer adsorption capacity (mg g^{-1}), K_L is the Langmuir equilibrium constant (L mg^{-1}), K_F is the Freundlich equilibrium constant ($(\text{mg g}^{-1}) \cdot (\text{mg L}^{-1})^{-1/n}$) and n is the adsorption strength. Finally, K_{RP} (L g^{-1}) and α_{RP} ($\text{L mg}^{-1})^\beta$ are the Redlich–Peterson constants, β is the Redlich–Peterson exponent ($\beta \leq 1$), q_{mLF} is the Langmuir–Freundlich maximum adsorption capacity (mg g^{-1}), K_{LF} (L mg^{-1}) is the Langmuir–Freundlich equilibrium constant and m_{LF} is the heterogeneity factor.

The equilibrium isotherm of CV on the KT belongs to type L, subgroup 1 (Fig. 8). The adsorption capacity at equilibrium increased with increasing initial CV concentration and reached a plateau gradually due to the high values of the initial CV concentration, possibly saturating the KT surface. The parameters of the four models used in this study are listed in Table 3.

The Freundlich model showed the lowest coefficient of determination ($R^2 = 0.936$); hence, multilayer adsorption on a heterogeneous surface is less plausible. The Langmuir model provided the best fit for the experimental data, with the highest coefficient of determination ($R^2 = 0.971$) being for the monolayer adsorption capacity ($q_m = 44.2 \text{ mg g}^{-1}$), which is very close to the experimental value obtained ($q_e = 41.9 \text{ mg g}^{-1}$). This result was also confirmed in the Redlich–Peterson model, because the Redlich–Peterson exponent was close to unity ($\beta = 0.941$). Therefore, this model was reduced in practical terms to the Langmuir model in the range of initial CV concentrations tested. The same result was also confirmed by the Langmuir–Freundlich model, in which the heterogeneity factor was also close to unity ($m_{LF} = 1.037$). Consequently, adsorption limited to a monolayer on a homogeneous surface without interactions between adsorbed molecules at the neighbouring sites can be proposed.

Thermodynamic study. To evaluate the thermodynamic parameters in terms of the adsorption of CV on the KT, various tests were carried out at three different temperatures (290, 303 and 313 K). Equations 12 and 13 were used to calculate the thermodynamic parameters (Puri *et al.*, 2018):

$$\ln(K_d) = -\frac{\Delta H^\circ}{RT} + \frac{\Delta S^\circ}{R} \quad (12)$$

Table 5. Maximum monolayer adsorption capacities of CV onto various adsorbents.

Adsorbent	Maximum adsorption capacity (mg g^{-1})	Reference
Calcined ball clay	40.80	Monsah <i>et al.</i> (2011)
Merck activated carbon	84.10	Sarabadan <i>et al.</i> (2019a)
Moroccan pyrophyllite	13.90	Miyah <i>et al.</i> (2017)
Acid-activated KT	50.50	Sarma <i>et al.</i> (2019)
Smectite	86.50	Hamza <i>et al.</i> (2018)
Zeolite–montmorillonite	150.50	Sarabadan <i>et al.</i> (2019a)
KT	24.75	Sargin <i>et al.</i> (2013)
Montmorillonite	370.40	Sharma <i>et al.</i> (2015)
Tamazert KT	44.20	Present study

$$\Delta G^\circ = \Delta H^\circ - T\Delta S^\circ \quad (13)$$

where K_d is the distribution coefficient, which is equal to q_e/C_e , ΔH° is the standard enthalpy of adsorption (kJ mol^{-1}), ΔS° is the standard entropy ($\text{J mol}^{-1} \cdot \text{K}^{-1}$), ΔG° is the Gibbs free energy of adsorption (kJ mol^{-1}), T is the absolute temperature (K) and R is the universal ideal gas constant ($\text{J K}^{-1} \text{mol}^{-1}$).

The calculated values of these parameters are reported in Table 4. The negative value of ΔH° indicates that the adsorption was exothermic due to the electrostatic forces between the electronic pairs on the silanol and aluminol groups and the positively charged molecules of the CV dye. In addition, the negative value of ΔG° suggests that the adsorption is spontaneous at the three temperatures tested. However, an increase in temperature led to an increase in ΔG° values, indicating that the adsorption was less favourable at greater temperatures. This suggests that weak forces govern the bond between the dye molecules and the electronic pairs of the hydroxyl groups, as was also confirmed by the low ΔH° value ($< 80 \text{ kJ mol}^{-1}$) and the ΔG° values ranging from 0 to -20 kJ mol^{-1} (Auta *et al.*, 2012).

Comparison with other adsorbents

The maximum adsorption capacity values of CV onto various adsorbents are listed in Table 5. The adsorption capacity of the KT was greater than those obtained from other raw and modified clay minerals reported in the literature (e.g. Monsah *et al.*, 2011; Sargin *et al.*, 2013; Miyah *et al.*, 2017). This can be attributed not only to the textural and structural properties of the KT, but also to its mineralogical composition. However, the efficiency of the KT remains lower than that reached by an undefined smectite (Hamza *et al.*, 2018) and montmorillonite (Sharma *et al.*, 2015) due to the lower CEC of the KT in comparison with those clay

minerals. Therefore, the KT can be considered suitable for CV dye removal due to its low cost and great availability.

Conclusions

We used a natural KT as an adsorbent for the removal of CV dye from aqueous solutions. This clay is characterized by a small specific surface area and low CEC. Nevertheless, it showed significant adsorption capacity due to its acidic and basic properties, which can be attributed to the presence of aluminol groups. Increasing the adsorbent dose, the initial pH and the stirring speed led to increases in the amount of adsorbed CV. However, increasing the temperature led to a decrease in the adsorption capacity, indicating the exothermic nature of this process. The adsorption was well described by the PSO model and the adsorption rate is controlled by external and intra-particle diffusion. Furthermore, the equilibrium study confirmed that adsorption was limited to a monolayer, as the adsorption isotherm is best described by the Langmuir model. The thermodynamic study confirmed the exothermic and the physical nature of the CV adsorption, which was favoured at lower temperatures. Weak forces bonded the dye molecules to the electronic pairs of the hydroxyl groups, low ΔH° values ($<80 \text{ kJ mol}^{-1}$) were obtained and the ΔG° values ranged from 0 to -20 kJ mol^{-1} . This study highlighted that this KT can be used as a low-cost and efficient adsorbent for the removal of CV dye. Additional research using other cationic dyes should be performed to evaluate the efficiency of this KT as an adsorbent. Furthermore, it would be interesting to test the efficiency of the adsorbent in a multicomponent system containing two or more dyes. Moreover, it is recommended that this study is cross-validated using non-linear equations to avoid systematic errors due to linearization.

Financial support. The authors were supported by the Spanish State Research Agency through the project PID2019-106186RB-I00/AEI/10.13039/50110001103 and by the Ministère Algérien de l'Enseignement Supérieur et de la Recherche Scientifique.

References

- Abbasi F., Yarak M.T., Farrokhnia A. & Bamdad M. (2020) Keratin nanoparticles obtained from human hair for removal of crystal violet from aqueous solution: optimized by Taguchi method. *International Journal of Biological Macromolecules*, **143**, 492–500.
- Abraham T., Lam N., Xu J., Zhang D., Whadhawan H., Kim H.J. *et al.* (2019) Collapse of house-of-cards clay structures and corresponding tailings dewatering induced by alternating electric field. *Drying Technology*, **37**, 1053–1067.
- Al-Bastaki N. (2004) Removal of methyl orange dye and Na_2SO_4 salt from synthetic waste water using reverse osmosis. *Chemical Engineering and Processing: Process Intensification*, **43**, 1561–1567.
- Al-Futaisi A., Jamrah A. & Al-Hanai R. (2007) Aspects of cationic dye molecule adsorption to palygorskite. *Desalination*, **214**, 327–342.
- Ali H. & Muhammad S.K. (2008) Biosorption of crystal violet from water on leaf biomass of *Calotropis procera*. *Journal of Environmental Science and Technology*, **1**, 143–150.
- Amari A., Chlendi M., Gannouni A. & Bellagi A. (2010) Optimised activation of bentonite for toluene adsorption. *Applied Clay Science*, **47**, 457–461.
- Askari N., Farhadian M., Razmjou A. & Hashtroodi H. (2016) Nanofiltration performance in the removal of dye from binary mixtures containing anthraquinones dyes. *Desalination and Water Treatment*, **57**, 18194–18201.
- Auta M. & Hameed B. H. (2012) Modified mesoporous clay adsorbent for adsorption isotherm and kinetics of methylene blue. *Chemical Engineering Journal*, 198–199, 219–227.
- Banerjee S., Dubey S., Guatam R.K., Chattopadhyaya M.C. & Sharma Y.C. (2019) Adsorption characteristics of alumina nanoparticles for the removal of hazardous dye, Orange G from aqueous solutions. *Arabian Journal of Chemistry*, **12**, 5339–5354.
- Belal R.M., Zayed M.A., El-Sherif R.M. & Abdel Ghani N.A. (2021) Advanced electrochemical degradation of basic yellow 28 textile dye using IrO_2/Ti meshed electrode in different supporting electrolytes. *Journal of Electroanalytical Chemistry*, **882**, 114979.
- Benhabiles S. & Rida K. (2021) Production of efficient activated carbon from sawdust for the removal of dyes in single and binary systems – a full factorial design. *Particulate Science and Technology*, **39**, 237–251.
- Boukhemkhem A. & Rida K. (2017) Improvement adsorption capacity of methylene blue onto modified Tamazert kaolin. *Adsorption Science and Technology*, **35**, 753–773.
- Boukhemkhem A., Rida K., Pizarro A.H., Molina C.B. & Rodriguez J.J. (2019) Iron catalyst supported on modified kaolin for catalytic wet peroxide oxidation. *Clay Minerals*, **54**, 67–73.
- Boukhemkhem A., Pizarro A.H. & Molina C.B. (2020) Enhancement of the adsorption properties of two natural bentonites by ion exchange: equilibrium, kinetics and thermodynamic study. *Clay Minerals*, **55**, 132–141.
- Bujdák J. (2020) Adsorption kinetics models in clay systems. The critical analysis of pseudo-second order mechanism. *Applied Clay Science*, **191**, 105630.
- Dargahzadeh M., Molaei M. & Karimipour M. (2018) Completely quenching of the trap states emission of CdS_eQDs by CdS/ZnS shell growth using a one pot photochemical approach and application for dye photo-degradation. *Journal of Luminescence*, **203**, 723–729.
- de Lima S.A., Murad M.A., Moyn C.A. & Stemmelen D. (2010) Three-scale model of pH-dependent flows and ion transport with equilibrium adsorption in kaolinite clays: I. Homogenization analysis. *Transport in Porous Media*, **85**, 23–44.
- Eren E. & Afsin E. (2007) Investigation of a basic dye adsorption from aqueous solution onto raw and pre-treated sepiolite surfaces. *Dyes and Pigments*, **73**, 162–167.
- Fabbri B., Gualtieri S. & Leonardi C. (2013) Modification induced by thermal treatment of kaolin and determination of reactivity of metakaolin. *Applied Clay Science*, **73**, 2–10.
- Feng H., Li C. & Shan H. (2009) Effect of calcination temperature of kaolin microspheres on the *in situ* synthesis of ZSM-5. *Catalysis Letters*, **129**, 71–78.
- Gadekar R.M. & Ahammed M.M. (2016) Coagulation/flocculation process for dye removal using water treatment residuals: modeling through artificial neural networks. *Desalination and Water Treatment*, **57**, 26392–26400.
- Geethakarathi A. & Phanikumar B.R. (2011) Adsorption of reactive dyes from aqueous solutions by tannery sludge developed activated carbon: kinetic and equilibrium studies. *International Journal of Environment Science and Technology*, **8**, 561–570.
- Giannakoudakis D.A., Kyzas G.Z., Avranas A. & Lazaridis N.K. (2016) Multi-parametric adsorption effects of the reactive dye removal with commercial activated carbons. *Journal of Molecular Liquids*, **213**, 381–389.
- Hachemaoui M., Boukoussa B., Mokhtar A., Mekki A., Beldjilali M., Benaissa M. *et al.* (2020) Dyes adsorption, antifungal and antibacterial properties of metal loaded mesoporous silica: effect of metal and calcination treatment. *Materials Chemistry and Physics*, **256**, 123704.
- Hamdaoui O. & Naffrechoux E. (2007) Modeling of adsorption isotherms of phenol and chlorophenols onto granular activated carbon. Part I. Two parameter models and equations allowing determination of thermodynamic parameters. *Journal of Hazardous Materials*, **147**, 381–394.
- Hamza W., Dammak N., Bel H., Eloussaief M. & Mourad B. (2018) Sono-assisted adsorption of crystal violet dye onto Tunisian smectite clay. *Ecotoxicology and Environmental Safety*, **163**, 365–371.
- Hassen H. & Hameed B.H. (2011) Fe-clay as effective heterogeneous Fenton catalyst for the decolorization of Reactive Blue 4. *Chemical Engineering Journal*, **171**, 912–918.
- Intachai S., Suppasso C. & Khaorapapong N. (2021) A novel process for intercalating alkylammonium ions in a Thai bentonite and its effect on adsorption performance. *Clays and Clay Minerals*, **69**, 477–488.
- Issa A.A., Al-Degs Y.S., Al-Ghouti M.A. & Olimat A.A.M. (2014) Studying competitive sorption behavior of methylene blue and malachite green using multivariate calibration. *Chemical Engineering Journal*, **240**, 554–564.

- Jiang M., Wang Q., Jin X. & Chen Z. (2009) Removal of Pb(II) from aqueous solution using modified and unmodified kaolinite clay. *Journal of Hazardous Materials*, **170**, 332–339.
- Jiang X., Zhang H., Yue M., Zhang S., Li Y. & Xu W. (2019) Synthesis of organic hybrid super-microporous silicas as an adsorbent for dyes removal from water. *Microporous and Mesoporous Materials*, **288**, 109598.
- Karatas D., Senol-Arslan D. & Ozdemir O. (2018) Experimental and atomic modeling of the adsorption of acid azo dye 57 to sepiolite. *Clays and Clay Minerals*, **66**, 426–437.
- Khairy M., Ayoub H.A., Rashwan F.A. & Abdel-Hafez H.F. (2018) Chemical modification of commercial kaolin for mitigation of organic pollutants in environment via adsorption and generation of inorganic pesticides. *Applied Clay Science*, **153**, 124–133.
- Konan K.L., Peyratout C., Smith A., Bonnet J.P., Rossignol S. & Oyetola S. (2009) Comparison of surface properties between kaolin and metakaolin in concentrated lime solutions. *Journal of Colloid and Interface Science*, **339**, 103–109.
- Kulkarni M.R., Revanth T., Acharya A. & Bhat P. (2017) Removal of crystal violet dye from aqueous solution using water hyacinth: equilibrium, kinetics and thermodynamics study. *Resource-Efficient Technologies*, **3**, 71–77.
- Kumar R. & Ahmed R. (2011) Biosorption of hazardous crystal violet dye from aqueous solution onto treated ginger waste (TGW). *Desalination*, **265**, 112–118.
- Li D., Yang Y., Li C. & Liu Y. (2017) A mechanistic study on decontamination of methyl orange dyes from aqueous phase by mesoporous pulp waste and polyaniline. *Environmental Research*, **154**, 139–144.
- Liew J., Wang Y., Fang Y., Mwamulima T., Song S. & Peng C. (2018) Removal of crystal violet and methylene blue from aqueous solutions using the fly ash-based adsorbent material-supported zero-valent iron. *Journal of Molecular Liquids*, **250**, 468–476.
- Lin J. & Wang L. (2009) Comparison between linear and non-linear forms of pseudo-first-order and pseudo-second-order adsorption kinetic models for the removal of methylene blue by activated carbon. *Frontiers of Environmental Science & Engineering*, **3**, 320–324.
- Li X., Li B., Xu J., Wang Q., Pang X., Gao X. *et al.* (2010) Synthesis and characterization of Ln-ZSM-5/MCM-41 (Ln = La, Ce) by using kaolin as raw material. *Applied Clay Science*, **50**, 81–86.
- Miklos D.B., Remy C., Jekel M., Linden K.G., Drewes J.E. & Hübner U. (2018) Evaluation of advanced oxidation processes for water and wastewater treatment: a critical review. *Water Research*, **139**, 118–131.
- Miyah Y., Lahrachi A., Idrissi M., Boujraf S., Taouda H. & Zerrouq F. (2017) Assessment of adsorption kinetics for removal potential of crystal violet dye from aqueous solutions using Moroccan pyrophyllite. *Journal of the Association of Arab Universities for Basic and Applied Sciences*, **23**, 20–28.
- Mobarak M., Selim A.Q., Mohammed E.A. & Selim M.K. (2018) A superior adsorbent of CTAB/H₂O₂ solution modified organic carbon rich-clay for hexavalent chromium and methyl orange uptake from solutions. *Journal of Molecular Liquids*, **259**, 384–397.
- Monash P., Niwas R. & Pugazhenthil G. (2011) Utilization of ball clay adsorbents for the removal of crystal violet dye from aqueous solution. *Clean Technology and Environmental Policy*, **13**, 141–151.
- Mouni L., Belkhir L., Bollinger J.C., Bouzaza A., Assadi A., Tirri A. *et al.* (2018) Removal of methylene blue from aqueous solutions by adsorption on kaolin: kinetic and equilibrium studies. *Applied Clay Science*, **153**, 38–45.
- Muayad E., Hubert R., Ahmed B., Hani K., Mohammed H. & Jan W. (2015) Development of inorganic polymer by alkali-activation of untreated kaolinitic clay: reaction stoichiometry, strength and dimensional stability. *Construction and Building Materials*, **91**, 251–259.
- Nadaroglu H., Kalkan E., Celebi N. & Tasgin E. (2015) Removal of Reactive Black 5 from wastewater using natural clinoptilolite modified with apolacase. *Clay Minerals*, **50**, 65–75.
- Nandi B.K., Goswami A., Das A.K., Mondal B. & Purkait M.K. (2008) Kinetic and equilibrium studies on the adsorption of crystal violet dye using kaolin as an adsorbent. *Separation Science and Technology*, **43**, 1382–1403.
- Nasuha N. & Hameed B.H. (2011) Adsorption of methylene blue from aqueous solution onto NaOH-modified rejected tea. *Chemical Engineering Journal*, **166**, 783–786.
- Pavan F.A., Gushikem Y., Mazzocato A.C., Dias S.L. & Lima E.C. (2007) Statistical design of experiments as tool for optimizing the batch conditions to methylene blue biosorption on yellow passion fruit and mandarin peels. *Dyes and Pigments*, **72**, 256–266.
- Puri G. & Sumana G. (2018) Highly effective adsorption of crystal violet dye from contaminated water using graphene oxide intercalated montmorillonite nanocomposite. *Applied Clay Science*, **166**, 102–112.
- Rezazadeh M., Baghdadi M., Mehrdadi N. & Abdoli M.A. (2021) Adsorption of crystal violet dye by agricultural rice bran waste: isotherms, kinetics, modeling and influencing factors. *Environmental Engineering Research*, **26**, 1–10.
- Rida K., Bouraoui S. & Hadnine S. (2013) Adsorption of methylene blue from aqueous solution by kaolin and zeolite. *Applied Clay Science*, **83–84**, 99–105.
- Rytwo G., Nir S. & Margulies L. (1993) Competitive adsorption of methylene blue and crystal violet to montmorillonite. *Clay Minerals*, **1**, 139–143.
- San Cristóbal A.G., Castelló R., Martín Luengo M.A. & Vizcayno C. (2010) Zeolites prepared from calcined and mechanically modified kaolins: a comparative study. *Applied Clay Science*, **49**, 239–246.
- Sarabadian M., Bashiri H. & Mousavi S.M. (2019a) Adsorption of crystal violet dye by a zeolite–montmorillonite nano-adsorbent: modelling, kinetic and equilibrium studies. *Clay Minerals*, **54**, 357–368.
- Sarabadian M., Bashiri H. & Mousavi S.M. (2019b) Removal of crystal violet dye by an efficient and low cost adsorbent: modelling, kinetic, equilibrium and thermodynamic studies. *Korean Journal of Chemical Engineering*, **36**, 1575–1586.
- Sarabadian M., Bashiri H. & Mousavi S.M. (2021) Modelling, kinetics and equilibrium studies of crystal violet adsorption on modified montmorillonite by sodium dodecyl sulfate and hyamine surfactants. *Clay Minerals*, **56**, 16–27.
- Sargin I. & Unlu N. (2013) Insights into cationic methyl violet 6B dye–kaolinite interactions: kinetic, equilibrium and thermodynamic studies. *Clay Minerals*, **48**, 85–95.
- Sarma G.K., Gupta S.S. & Bhattacharyya G.G. (2019) Removal of hazardous basic dyes from aqueous solution by adsorption onto kaolinite and acid-treated kaolinite: kinetics, isotherm and mechanistic study. *SN Applied Sciences*, **1**, 211.
- Sharma P., Kaur H., Sharma M. & Sahore V. (2011) A review on applicability of naturally available adsorbents for the removal of hazardous dyes from aqueous waste. *Environmental Monitoring and Assessment*, **183**, 151–195.
- Sharma P., Borah D.J., Das P. & Das M.R. (2015) Cationic and anionic dye removal from aqueous solution using montmorillonite clay: evaluation of adsorption parameters and mechanism. *Desalination and Water Treatment*, **57**, 8372–8388.
- Srinivasan S. & Sadavisam S.K. (2021) Biodegradation of textile azo dyes by textile effluent non-adapted and adapted *Aeromonas hydrophila*. *Environmental Research*, **194**, 110643.
- Thommes M., Kaneko K., Neimark A.V., Olivier J.P., Rodriguez-Reinoso F., Rouquerol J. & Sing K.S.W. (2015) Physisorption of gases, with special reference to the evaluation of surface area and pore size distribution (IUPAC Technical Report). *Pure and Applied Chemistry*, **87**, 1051–1069.
- Varjani S., Rakholiya P., Ng H.Y., You S. & Teixeira J.A. (2020) Microbial degradation of dyes: an overview. *Bioresource Technology*, **314**, 123728.
- Vishwakarma M.C., Tiwari P., Joshi S.K., Sharma H. & Bhandari N.S. (2018) Adsorption of Cu(II) ion onto activated *Eupatorium adenophorum* and *Acer oblongum*; thermodynamic, kinetics and equilibrium studies. *Chemical Science Transactions*, **7**, 445–463.
- Volzone C. & Ortega J. (2006) Removal of gases by thermal-acid leached kaolinitic clays: influence of mineralogical composition. *Applied Clay Science*, **32**, 87–93.
- Xia Y., Azaiez J. & Hill J.M. (2018) Erroneous application of pseudo-second-order adsorption kinetics model: ignored assumptions and spurious correlations. *Industrial & Engineering Chemistry Research*, **57**, 2705–2709.
- Yagub M.T., Sen T.K., Afroz S. & Ang H.M. (2014) Dye and its removal from aqueous solution by adsorption: a review. *Advances in Colloid and Interface Science*, **209**, 172–184.
- Yaseen D.A. & Scholz M. (2019) Textile dye wastewater characteristics and constituents of synthetic effluents: a critical review. *International Journal of Environmental Sciences and Technology*, **16**, 1193–1126.